An Improved Deadbeat Predictive Stator Flux Control with Reduced-Order Disturbance Observer for In-Wheel PMSMs

Xiaodong Sun, *Senior Member, IEEE*, Yao Zhang, Gang Lei, *Member, IEEE*, Youguang Guo, *Senior Member, IEEE*, and Jianguo Zhu, *Senior Member, IEEE*

***Abstract*—In this paper, an improved deadbeat predictive stator flux control (DPSFC) based on disturbance observer is proposed to address the problems of the steady state tracking error and robustness decrease due to the detrimental parameter mismatch and disturbance. Firstly, the sensitivity of conventional deadbeat predictive current control to the parameter variation, including flux linkage, stator inductance and resistance, is analyzed. Then, a reduced-order observer based on additional disturbance state variables in discrete time is designed to predict the future stator flux and observe the system disturbance caused by parameter mismatch. The proposed DPSFC method is able to enhance the robustness of the drive performance effectively via applying the estimated disturbance as the feed-forward compensations of one-step delay and stator voltage. Additionally, the theoretical proof is given. Finally, the superiority of the proposed control method is validated by simulations and experiments on a prototype of an in-wheel permanet magnet synchronous motor (PMSM) drive.**

***Index Terms*—Deadbeat predictive stator flux control, permanent magnet synchronous motors (PMSMs), parameter mismatch, disturbance observer.**

I. Introduction

A. Motivation

PERMANENT magnet synchronous motors (PMSMs) have been employed in various industrial applications due to several advantages like high-power density, high efficiency, compact structure and fast dynamic response. However, the performance of PMSMs will deteriorate when the irreversible demagnetization resulted from the violent vibration, ultra-high temperature (for NdFeB permanent magnet), or ultra-low temperature (for ferrite permanent magnet) exists [1]-[6]. Different from internal-rotor PMSMs, the in-wheel PMSMs with external rotors integrate the drive, transmission and braking devices into the hub and can avoid the use of a series of mechanical parts such as clutch and transmission [7]-[10]. The in-wheel PMSMs are also easier to achieve braking energy recovery, and hence occupy an important position in the development of automotive energy-saving technology. However, the control system of the in-wheel PMSMs is nonlinear, strongly coupled and multivariable. The control method is of crucial importance to system performance. Based on the typical double-loop structure, the outer loop is to regulate rotor speed, whereas the inner loop is to control stator current, tracking the reference current. In order to obtain high precision and fast dynamic response, many control methods have been introduced in the inner loop, such as hysteresis control [11], sliding mode control [12] and predictive control [13]-[17].

The hysteresis control is a simple control method with good robustness. It can speed up the dynamic adjustment and suppress the disturbance in the loop, which is not much dependent on the parameters of the motor. However, the variable switching frequency of the inverter will lead to a large pulsation of the output current and huge noise inside the motor [18]. The fuzzy control is applicable to nonlinear systems and does not depend on the precise mathematical model of the controlled object. However, when the nonlinearity and uncertainty of the system are serious, the control performance will deteriorate [19]. Among these control schemes, the predictive control method has received considerable attention in recent years due to several merits such as simple implementation, great steady-state and dynamic performance.

B. Related Research

The conventional model predictive control (MPC) finds the optimal voltage vector which minimizes the cost function [17]. Model predictive current control (MPCC) and model predictive

Manuscript received Sep 17, 2020; revised Jan 02, 2021; accepted Mar 22, 2021. This work was supported by the National Natural Science Foundation of China under Project 51875261, the Natural Science Foundation of Jiangsu Province of China under Project BK20180046, and the "Qinglan project" of Jiangsu Province. *(Corresponding author: Gang Lei)*

X. Sun and Y. Zhang are with the Automotive Engineering Research Institute, Jiangsu University, Zhenjiang 212013, China (email: xdsun@ujs.edu.cn, 18852852927@163.com,).

G. Lei and Y. Guo are with the School of Electrical and Data Engineering, University of Technology Sydney, NSW 2007, Australia (e-mail: Gang.Lei@uts.edu.au, Youguang.Guo-1@uts.edu.au).

J. Zhu is with the School of Electrical and Information Engineering, University of Sydney, NSW, 2006, Australia (e-mail: jianguo.zhu@sydney.edu.au).

torque control (MPTC) are popular among MPC methods [20]-[23]. Due to the existence of deviation between the optimal voltage vector and reference voltage vector, the static characteristic of the system and switching frequency will be affected. In [24], an improved MPCC method based on incremental model was proposed to improve the anti-disturbance capability of the system, but it results in a heavy computation. In order to deal with high computation burden in MPC, a new MPC method based on deadbeat control was proposed [25]-[28].

In contrast to the MPC method, the deadbeat predictive control (DPC) method calculates the voltage reference during every sampling period and translates it into a switching signal through pulse width modulation (PWM) technology. Therefore, the DPC method has the potential of faster dynamic response, better tracking performance and less computational effort. Nowadays, DPC methods have been adopted for the inner loop in many industrial areas. However, the performance of DPC method relies on precise models. In practice, magnetic flux linkage changes with rotor permanent magnet temperature, and the magnetic flux density in the stator iron core changes as well. This magnetic flux density in the stator iron core changes the permeability of the magnetic flux path, and hence it also changes
inductances [29]. When the motor parameters mismatch due to the temperature rise, magnet demagnetization and other faults, the robustness of the control will decrease especially for the in-wheel PMSM whose heat dissipation performance in the narrow hub is poor. Moreover, the one-step delay in digital control like sampling delay is not avoidable, which will also deteriorate the control performance. In order to address these problems, some methods have been proposed [30]-[33].

In [30], an improved deadbeat predictive current control (DPCC) method with parameter identification was proposed. The zero steady-state current error is eliminated, and the ideal dynamic current response could be achieved. The effectiveness can be guaranteed at both low- and high-frequency by establishing a fully-discretized model. The expected voltage resulted from parameter mismatch and current error in conventional DPCC will amplify the torque ripple and speed fluctuation. In [31], an accurate PMSM model with aperiodic and periodic disturbances was established, and a novel current and disturbance observer was proposed. In [32], in order to promote the control performance, a unified high-order sliding mode observer was designed for the DPCC method. Both parameters and external disturbances in the speed and current loops can be estimated by the sliding mode observer and feedbacked to the DPCC method. In this way, the speed robustness and current tracking accuracy can be improved. In general, the sensitivities to disturbances and delays will be increased at low switching frequency due to long delays and larger errors in the discretization of the model. A novel DPCC method in $\alpha\beta$-axis with a moving horizon estimator was investigated in [33]. The back electromotive force (EMF) and parameter variations are estimated by the moving horizon estimator and are considered as compensations. As a result, the robustness of the system at low switching frequency can be increased significantly.

C. Contributions

The permanent magnet flux linkage and inductance may change due to temperature rise and magnet saturation, especially under high-temperature operation conditions. In view of the fact that the traditional DPCC method relies on precise models and is very sensitivie to parameter perturbations, the challenges of the traditional DPCC method is how to suppress the disturbance caused by the parameter perturbations. To overcome the aforementioned drawbacks in the traditional DPCC, in this paper, an improved deadbeat predictive stator flux control (DPSFC) method is developed to improve the performance of PMSM drives when parameter perturbations and one-step delay exist in digital control. Furthermore, the proposed DPSFC method is able to enhance the robustness of the drive performance effectively via the compensations of one-step delay and stator voltage.

The main contributions of the proposed scheme can be listed as:

1) The improved DPSFC method can retain the fast dynamic response of the conventional DPCC.
2) A reduced-order observer based on state flux state is designed in discrete time to observe the system disturbance caused by parameter mismatch. Applying the estimated disturbance as the feed-forward compensations for stator voltage, the tracking error between the actual response and its reference can be narrowed effectively.
3) The proposed DPSFC method based on the state space structure reduces the calculation burden of the nonlinear system.
4) One-step delay compensation is also considered in the DPSFC design to improve the control accuracy, which is ignored by the traditional DPCC scheme.

D. Paper Organization

The rest of this paper is organized as follows. A nonlinear PMSM model considering parameter mismatch is developed in Section II. The influence of model parameter mismatch on conventional DPCC is analyzed in Section III. The DPSFC method with disturbance observer is proposed in Section IV. The simulation and experiment results are provided in Sections V and VI, respectively, followed by the conclusion.

II. Mathematical Model of PMSMs

For surface-mounted permanent magnet synchronous motor (SPMSM), stator inductance L_d=L_q=L_s. Under the synchronous rotating coordinate d-q, the stator voltage equation of the PMSMs can be described as

$$\begin{cases} u_d = R_s i_d + L_s \dfrac{di_d}{dt} - \omega_e L_s i_q \\ u_q = R_s i_q + L_s \dfrac{di_q}{dt} + \omega_e L_s i_d + \omega_e \psi_f \end{cases} \tag{1}$$

The flux linkage equation is

$$\begin{cases}\psi_d = L_d i_d + \psi_f \\ \psi_q = L_q i_q\end{cases} \tag{2}$$

where u_d, u_q, i_d, and i_q are the d- and q-axis components of the stator voltage, and current in the d-q reference frame, respectively. R_s and ψ_f are the stator resistance and the magnetic flux of the SPMSM, respectively. ω_e is the electrical angular speed of the rotor.

According to (1) and (2), the augmented state equation of PMSM considering disturbance can be transformed to (3), where f_d and f_q denote the disturbances caused by the parameter variations in the d-axis and q-axis, respectively.

$$\begin{cases}u_d = \dfrac{d\psi_d}{dt} + \dfrac{R_s}{L_s}\psi_d - \omega_e\psi_q + f_d - \dfrac{R_s}{L_s}\psi_f \\ u_q = \dfrac{d\psi_q}{dt} + \omega_e\psi_d + \dfrac{R_s}{L_s}\psi_q + f_q\end{cases} \tag{3}$$

The mechanical equation of motion of the motor can be expressed as

$$\begin{cases}\dfrac{d\omega_m}{dt} = \dfrac{1}{J}\left(T_e - T_L - \nu\omega_m\right) \\ T_e = \dfrac{3}{2}p_n i_q \psi_f\end{cases} \tag{4}$$

where ω_m is the mechanical angular speed of the rotor, p_n the number of pole pairs, ν the viscous friction coefficient, and J the overall rotor inertia. T_e and T_L are the electromagnetic torque and the mechanical torque, respectively.

III. Parameter Sensitivity Analysis on Conventional Deadbeat Predictive Current Control

The conventional DPCC is a discrete model control algorithm based on the specific model. The control performance is closely associated with the parameter mismatches, including stator inductance L_s, stator resistance R_s and permanent magnetic flux linkage ψ_f because of temperature or other external factors. In order to evaluate the relationship between parameter mismatch and DPCC, the parameter sensitivity to conventional DPCC is focused in this section. Fig. 1 illustrates a control diagram for the conventional DPCC method.

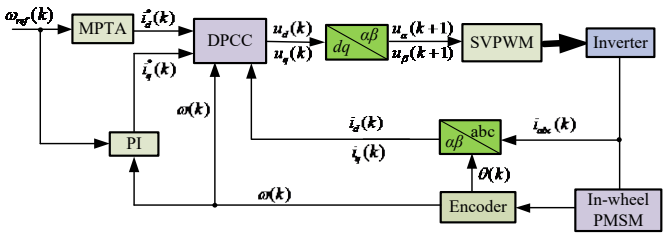

Fig. 1. Diagram of the conventional DPCC.

According to (1), the discrete current predictive model of in-wheel PMSMs with parameter disturbance can be described as follows.

$$\begin{bmatrix}i_d(k+1) \\ i_q(k+1)\end{bmatrix} = E_0(k)\cdot\begin{bmatrix}i_d(k) \\ i_q(k)\end{bmatrix} + F_0\cdot\begin{bmatrix}u_d(k) \\ u_q(k)\end{bmatrix} + G_0(k) \tag{5}$$

where

$$E_0(k) = \begin{bmatrix}1 - \dfrac{T_s R_s}{L_s} & T_s\omega_e(k) \\ -T_s\omega_e(k) & 1 - \dfrac{T_s R_s}{L_s}\end{bmatrix} \quad F_0 = \begin{bmatrix}\dfrac{T_s}{L_s} & 0 \\ 0 & \dfrac{T_s}{L_s}\end{bmatrix}$$

$$G_0(k) = \begin{bmatrix}0 \\ -\dfrac{T_s\psi_f}{L_s}\omega_e(k)\end{bmatrix}$$

In conventional DPCC method, the output voltage of the predictive controller at the kT_s moment can be obtained as follows [34]:

$$\begin{bmatrix}u_d(k) \\ u_q(k)\end{bmatrix} = F^{-1}\left\{\begin{bmatrix}i_d^{ref}(k+1) \\ i_q^{ref}(k+1)\end{bmatrix} - E(k)\cdot\begin{bmatrix}i_d(k) \\ i_q(k)\end{bmatrix} - G(k)\right\} \tag{6}$$

where $i_d^{ref}(k+1)$ and $i_q^{ref}(k+1)$ are the reference currents.

According to (5), (6) can be expressed as

$$\begin{bmatrix}i_d^{ref}(k+1) \\ i_q^{ref}(k+1)\end{bmatrix} = E(k)\cdot\begin{bmatrix}i_d(k) \\ i_q(k)\end{bmatrix} + F\cdot\begin{bmatrix}u_d(k) \\ u_q(k)\end{bmatrix} + G(k) \tag{7}$$

where

$$E(k) = \begin{bmatrix}1 - \dfrac{T_s R_s'}{L_s'} & T_s\omega_e(k) \\ -T_s\omega_e(k) & 1 - \dfrac{T_s R_s'}{L_s'}\end{bmatrix} \quad F = \begin{bmatrix}\dfrac{T_s}{L_s'} & 0 \\ 0 & \dfrac{T_s}{L_s'}\end{bmatrix}$$

$$G(k) = \begin{bmatrix}0 \\ -\dfrac{T_s\psi_f'}{L_s'}\omega_e(k)\end{bmatrix}$$

where $R_s' = R_s + \nabla R_s$, $L_s' = L_s + \Delta L_s$, $\psi_f' = \psi_f + \Delta\psi_f$, ΔR_s, ΔL_s and /Wb$\Delta\psi_f$ are the variations of resistance, inductance and permanent magnet flux linkage from their true values.

At the $(k+1)T_s$ moment, the voltage vector at the sampling period k is applied due to the sampling delay. Substituting (7) into (2) yields

$$\begin{bmatrix}i_d(k+1) \\ i_q(k+1)\end{bmatrix} = \begin{bmatrix}i_d^{ref}(k+1) \\ i_q^{ref}(k+1)\end{bmatrix} + \begin{bmatrix}e_d(k) \\ e_q(k)\end{bmatrix} \tag{8}$$

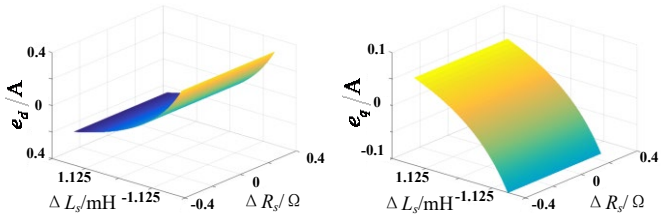

(a) (b)

Fig. 2. d- and q-axis current errors under inductance and resistance mismatch (error range: ±50%): (a) d-axis current error, and (b) q-axis current error.

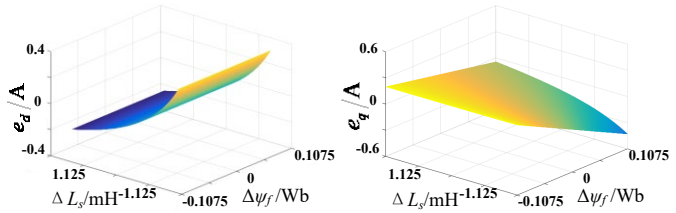

(a) (b)

Fig. 3. *d*- and *q*-axis current errors under inductance and permanent magnet flux mismatch (error range: ±50%): (a) *d*-axis current error, and (b) *q*-axis current error.

From (8), there exists a current error between the current response $i_d(k+1)$, $i_q(k+1)$ and the current reference vector $i_d^{ref}(k+1)$, $i_q^{ref}(k+1)$ subjected to model parameter mismatch (stator inductance, stator resistance and flux linkage of permanent magnets). The current error can be expressed as follows.

$$\begin{cases} e_d(k) = i_d^{ref}(k+1) - i_d(k+1) = -\dfrac{T_s R_s \Delta L_s - T_s \Delta R_s L_s}{L_s L_s} i_d(k) \\ \qquad + \dfrac{T_s \Delta L_s}{L_s L_s} u_d(k) \\ e_q(k) = i_q^{ref}(k+1) - i_q(k+1) = -\dfrac{T_s R_s \Delta L_s - T_s \Delta R_s L_s}{L_s L_s} i_q(k) \\ \qquad + \dfrac{T_s \Delta L_s}{L_s L_s} u_q(k) - \dfrac{T_s \omega_e \psi_f \Delta L_s - T_s \omega_e \Delta \psi_f L_s}{L_s L_s} \end{cases} \tag{9}$$

Table I lists some main parameters for the investigated in-wheel PMSM. When parameter perturbations occur, the *d*- and *q*- axis current errors can be plotted, as shown in Figs. 2&3. The error ranges of these three parameters are set to be ±50% of the original values. Fig. 2 indicates the current errors of *d*-and *q*-axis with induction and resistance mismatches. The current errors of both *d*-and *q*-axis resulted from resistance perturbation can be neglected. Furthermore, the inductance mismatch has a significant impact on current errors. Fig. 3 shows the current errors of *d*-and *q*-axis under inductance and permanent magnet flux linkage errors. The permanent magnet flux linkage mismatch has no influence on *d*-axis current while it does affect the *q*-axis current, which also can be seen from (9).

TABLE I
MAIN PARAMETERS OF AN IN-WHEEL PMSM

Parameter	Symbol	Value
No. of pole pairs	P	22
Stator resistance	R_s	0.8 Ω
d-axis inductance	L_s	4.5 mH
q-axis inductance	L_s	4.5 mH
Permanent-magnet flux linkage	ψ_f	0.215 Wb
Inertia	J	0.03 kgm^2
Rated speed	N	360 rpm
Rated power	P_N	30 kW

Through the above analysis, it can be concluded that the conventional DPCC is very sensitive to inductance and flux linkage, while the influence of stator resistance can be neglected. In order to overcome the negative influence of model parameter mismatches, a DPSFC with disturbance observer is proposed.

IV. DPSFC WITH DISTURBANCE OBSERVER

When the inductance mismatch and permanent magnet demagnetization occur, the control performance will deteriorate unless the corresponding compensation method is applied to suppress it. Meanwhile, the existence of one-step delay will degrade the control performance in the digital control system if this problem is not taken into account in the design. This section presents an improved DPSFC with disturbance observer against these two factors. First, a disturbance observer is proposed in subsection A. The stability analysis of the proposed disturbance observer is shown in subsection B. Using the observer, the future value of stator flux can be predicted, and the system disturbance caused by parameter mismatch can be tracked simultaneously. Then, the DPSFC control method based on the disturbance observer is proposed and its effectiveness in theory is analyzed in subsection C.

A. The Proposed Disturbance Observer

In order to estimate the disturbance caused by parameter mismatch, a reduced-order observer is adopted, in which the feedback of disturbance is utilized to compensate voltage, as illustrated in Fig. 4. According to (1) and (2), the augmented state equation of in-wheel PMSMs considering the disturbance caused by parameter mismatch can be transformed to

$$\begin{cases} \dfrac{d\psi_d(k)}{dt} = -\dfrac{R_s}{L_s}\psi_d(k) + \omega_e(k)\psi_q(k) - f_d(k) + u_d(k) + \dfrac{R_s}{L_s}\psi_f \\ \dfrac{d\psi_q(k)}{dt} = -\omega_e(k)\psi_d(k) - \dfrac{R_s}{L_s}\psi_q(k) - f_q(k) + u_q(k) \end{cases} \tag{10}$$

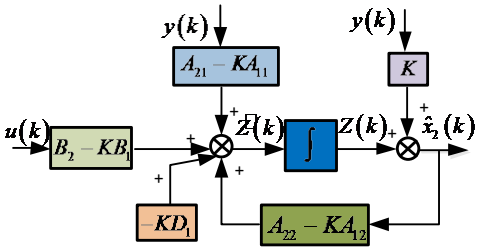

Fig. 4. Diagram of the proposed disturbance observer.

Since the disturbance f_d, f_q cannot be obtained in the conventional DPCC scheme, fd and fq can be regarded as additional state variables. Applying that fd=0 and fq=0, $\dot{f}_d = 0$ and $\dot{f}_q = 0$, the augmented state equation can be described as follows.

$$\begin{bmatrix} \dot{x}_1(k) \\ \dot{x}_2(k) \end{bmatrix} = \begin{bmatrix} A_{11} & A_{12} \\ A_{21} & A_{22} \end{bmatrix} \begin{bmatrix} x_1(k) \\ x_2(k) \end{bmatrix} + \begin{bmatrix} B_1 \\ B_2 \end{bmatrix} u(k) + \begin{bmatrix} D_1 \\ D_2 \end{bmatrix} \tag{11}$$

$$y(k) = C \begin{bmatrix} x_1(k) \\ x_2(k) \end{bmatrix} \tag{12}$$

where $x_1(k)=[\psi_d(k),\ \psi_q(k)]^T$, $x_2(k)=[f_d(k),\ f_q(k)]^T$, $A_{11}=[-R_s/L_s,\ \omega_e(k);\ -\omega_e(k),\ -R_s/L_s]$, $A_{12}=[-1,\ 0;\ 0,\ -1]$, $A_{21}=A_{22}=[0,\ 0;\ 0,\ 0]$, $B_1=[1,\ 0;\ 0,\ 1]$, $B_2=[0,\ 0;\ 0,\ 0]$, $C=[I,\ 0]$, $D_1=[R_s\psi_f/L_s;\ 0]$, $D_2=[0;\ 0]$

According to (11) and (12), the two subsystems can be expressed as follows.

$$\begin{cases} \dot{y}(k)=A_{11}y(k)+A_{12}x_2(k)+B_1u(k)+D_1 \\ \dot{x}_2(k)=A_{22}x_2(k)+A_{21}y(k)+B_2u(k) \\ \qquad =A_{22}x_2(k)+\begin{bmatrix}A_{21} & B_2\end{bmatrix}\begin{bmatrix}y(k)\\u(k)\end{bmatrix} \end{cases} \tag{13}$$

Equation group (14) can be obtained as follows based on the definition (15).

$$\begin{cases} \dot{x}_2(k)=A_{22}x_2(k)+B'u'(k) \\ \bar{y}(k)=A_{12}x_2(k) \end{cases} \tag{14}$$

$$\begin{cases} B'=\begin{bmatrix}A_{21} & B_2\end{bmatrix} \\ u'(k)=\begin{bmatrix}y(k)\\u(k)\end{bmatrix} \\ \bar{y}(k)=\dot{y}(k)-A_{11}y(k)-B_1u(k)-D_1 \end{cases} \tag{15}$$

Since B', $u'(k)$ and $\bar{y}(k)$ in (15) are available, the system based on (14) is completely observable and all the subsystems are also observable. Therefore, to estimate state variable $x_2(k)$, a reduced-order observer can be designed as (16), where K is an observer gain matrix which can assign the poles of the matrix $(A_{22}\text{-}KA_{12})$.

$$\dot{\hat{x}}_2(k)=(A_{22}-KA_{12})\hat{x}_2(k)+K\bar{y}(k)+B'u'(k) \tag{16}$$

B. *Stability Analysis of the Disturbance Observer*

The error is chosen as $e(k)=x_2(k)-\hat{x}_2(k)$, and the error dynamics of the observer can be described as

$$\dot{e}(k)=(A_{22}-KA_{12})e(k) \tag{17}$$

According to the classical control theory, some main performance indexes of the closed-loop system are basically determined by the position of the system poles on the complex plane. It is desirable that the estimated state should follow the actual state closely with a good dynamic response (the error is zero). Meanwhile, the system poles are assigned by the gain matrix K to ensure the eigenvalues of $(A_{22}\text{-}KA_{12})$ to have negative real parts. Therefore, the choice of an appropriate gain matrix K is of great significance. The eigenvalues of the matrix $(A_{22}\text{-}KA_{12})$ is as follows:

$$\det\left|sI-(A_{22}-KA_{12})\right|=s^2-(K_1+K_4)s+K_1K_4-K_2K_3=0 \tag{18}$$

From the classical control theory, the second-order characteristics equation is given as

$$\Delta=s^2+2\zeta\omega_n s+\omega_n^2=0 \tag{19}$$

The observer poles can be easily obtained.

$$s_{1,2}=-\zeta\omega_n\pm\omega_n\sqrt{\zeta^2-1} \tag{20}$$

where $\omega_n=\sqrt{K_1K_4-K_2K_3}$, $\zeta=-\dfrac{K_1+K_4}{2\sqrt{K_1K_4-K_2K_3}}$.

Hence, the eigenvalues of the matrix $(A_{22}\text{-}KA_{12})$ can be suitably assigned in the left half of s-plane so that the estimated state approaches the actual state asymptotically.

The implementation of the observer in (16) requires the differentiator for the derivative of $y(k)$, which is unacceptable as it amplifies the noise due to quantization and measurement. Considering that differentiators are difficult to implement and the approximate differentiators may cause high-frequency interference, the elimination method is adopted in practice. Substituting (15) back into (16) yields

$$\begin{aligned} \dot{\hat{x}}_2(k)-K\dot{y}(k)&=(A_{22}-KA_{12})\hat{x}_2(k)+(A_{21}-KA_{11})y(k) \\ &+(B_2-KB_1)u(k)-KD_1 \end{aligned} \tag{21}$$

Regarding $\dot{\hat{x}}_2(k)-K\dot{y}(k)$ as a whole in (22), the derivative of $y(k)$ is eliminated. Then, in terms of this state, the disturbance observer is described as (23):

$$\begin{cases} Z(k)=\hat{x}_2(k)-Ky(k) \\ \dot{Z}(k)=\dot{\hat{x}}_2(k)-K\dot{y}(k) \end{cases} \tag{22}$$

$$\begin{aligned} \dot{Z}(k)&=(A_{22}-KA_{12})Z(k)+(B_2-KB_1)u(k)-KD_1 \\ &+[(A_{22}-KA_{12})K+(A_{21}-KA_{11})]y(k) \end{aligned} \tag{23}$$

The estimated state can be obtained from the dummy state variable $Z(k)$, as follows

$$\hat{x}_2(k)=Z(k)+Ky(k) \tag{24}$$

To obtain the stability and convergence of the observer, the value of the observer gain matrix $K=[k_1,k_2;k_3,k_4]^T$ is obtained as follows: $K_1=$-400, $K_2=$400, $K_3=$-400, and $K_4=$ -400. As shown in Fig. 5 with the zoomed-in estimated disturbance plots, when there exists no parameter mismatch, the estimated disturbance is steady at 0V; when parameter mismatch occurs at 0.1 s, the disturbance observer generates an observed value of -40 V for compensation which demonstrates a fast convergence and stability.

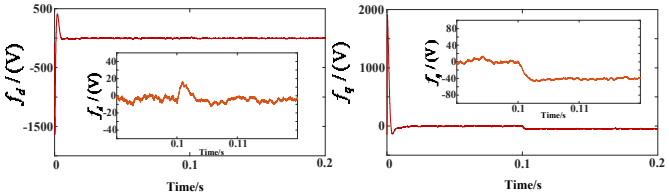

(a) (b)

Fig. 5. The d- and q-axes disturbances estimated by the disturbance observer under parameter mismatch: ΔL_s=-0.5L_s.

C. *DPSFC Method with Disturbance Observer*

The form of formula (11) can be simplified as (25) when the disturbance cannot be obtained in the conventional DPCC method:

$$\dot{x}=Ax+Bu+D \tag{25}$$

Fig. 6. shows the conventional DPCC diagram and its simplification in the discrete domain. The system transfer function can be derived as

$$G(z)=\frac{G_1(z)G_2(z)z^{-1}G_3(z)}{I+G_2(z)z^{-1}G_3(z)}=z^{-2} \tag{26}$$

where $G_1(z)=(I+AT_s)^{-2}$, $G_2(z)=(I+AT_s)^2(zI+I+AT_s)^{-1}(BT_s)^{-1}z$, $G_3(z)=BT_s[zI-(I+AT_s)]^{-1}$.

The conventional DPCC can obtain the fast dynamic response due to the two-sample deadbeat control. However, the disturbance f must be considered when the inevitable parameter mismatches occur in practice. The error transfer function is as follows:

$$G_e(z)=\frac{e(z)}{f(z)}=\frac{G_3(z)}{1+G_2(z)z^{-1}G_3(z)} \tag{27}$$

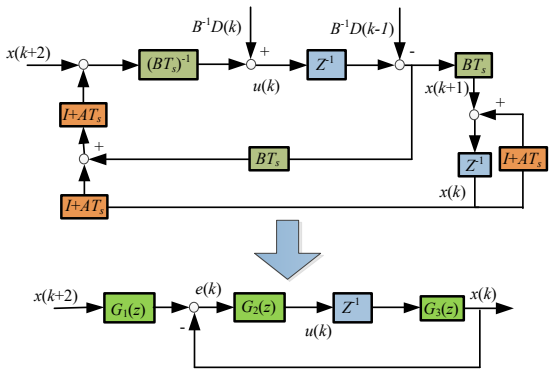

Fig. 6. Diagram of the conventional DPCC and its simplification form in the discrete domain.

Provided that the disturbance is a step-function signal, the steady state error caused by the disturbance based on the final-value theorem can be expressed as

$$e(\infty)=\lim_{z\to 1}\frac{zI-I}{zI}G_e(z)f(z)=\frac{2BT_s}{I-AT_s} \tag{28}$$

Formula (28) indicates the unavoidable error in the conventional DPCC when the disturbance caused by the parameter mismatches exists.

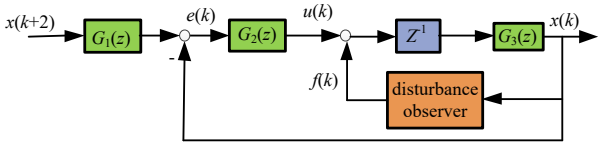

Fig. 7. Diagram of the proposed DPSFC with disturbance observer in the discrete domain.

According to (3) and (9), the discrete deadbeat predictive model of PMSM under parameter mismatch can be expressed as follows

$$\begin{bmatrix}u_d(k)\\u_q(k)\end{bmatrix}=\begin{bmatrix}R_s/L_s-1/T_s & -\omega_e(k)\\ \omega_e(k) & R_s/L_s-1/T_s\end{bmatrix}\begin{bmatrix}\hat{\psi}_d(k)\\\hat{\psi}_q(k)\end{bmatrix}+\begin{bmatrix}\psi_d(k+1)/T_s\\\psi_q(k+1)/T_s\end{bmatrix}+\begin{bmatrix}-R_s\cdot\psi_f/L_s\\0\end{bmatrix}+\begin{bmatrix}f_d(k)\\f_q(k)\end{bmatrix} \tag{29}$$

There always exists inevitable time delay in a discrete system including signal sampling delay, computation delay, execution delay, duty cycle refreshing delay or some other factors. When the calculated voltages are operated in control, the actual rotor position has rotated by an angle due to the time delay. This leads to the inaccurate steady-state current tracking and instability of the control system. In order to compensate for the one-step delay, $u_d(k+1)$ and $u_q(k+1)$ should be calculated by obtaining predictive flux values $\psi_d(k+1)$ and $\psi_q(k+1)$ at the k-th moment. In other words, replacing $\psi_d(k)$, $\psi_q(k)$ with predictive stator flux $\psi_d(k+1)$, $\psi_q(k+1)$ can reduce the influence on control performance. Since the electromagnetic time constant is much smaller than the mechanical time constant in the motor system, the rotor speed can be considered as constant during one sampling period, $\omega_e(k)=\omega_e(k+1)$; setting $\psi_{dq}^{ref}(k)=\psi_{dq}(k+2)$, (29) can be modified into (30), where '^' denotes predictive values.

$$\begin{bmatrix}u_d(k+1)\\u_q(k+1)\end{bmatrix}=\begin{bmatrix}R_s/L_s-1/T_s & -\omega_e(k)\\ \omega_e(k) & R_s/L_s-1/T_s\end{bmatrix}\begin{bmatrix}\hat{\psi}_d(k+1)\\\hat{\psi}_q(k+1)\end{bmatrix}+\begin{bmatrix}\psi_d^{ref}(k)/T_s\\\psi_q^{ref}(k)/T_s\end{bmatrix}+\begin{bmatrix}-R_s\cdot\psi_f/L_s\\0\end{bmatrix}+\begin{bmatrix}f_d(k+1)\\f_q(k+1)\end{bmatrix} \tag{30}$$

According to Fig. 7, the error transfer function is as follows:

$$\hat{G}_e(z)=\frac{e(z)}{f(z)}=\frac{z^{-1}G_3(z)}{1+G_2(z)z^{-1}G_3(z)}=-z^{-1}G_e(z) \tag{31}$$

The steady state error of the proposed DPSFC method with disturbance observer can be expressed as

$$\hat{e}(\infty)=\lim_{z\to 1}[\frac{zI-I}{zI}G_e(z)z^{-1}f(z)+\frac{zI-I}{zI}\hat{G}_e(z)f(z)]=0 \tag{32}$$

Fig. 8 shows a block diagram of the DPSFC with disturbance observer. The predicted stator flux from the disturbance observer is applied to compensate for the one-step delay caused by the digital controller. The estimated disturbance is regarded as a feedforward to make up for the voltage reference calculated by DPSFC controller. Based on the formula (32), the proposed scheme can eliminate the error theoretically. The robustness of the system can be improved by applying compensations of the disturbance caused by the parameter mismatch and the one-step delay.

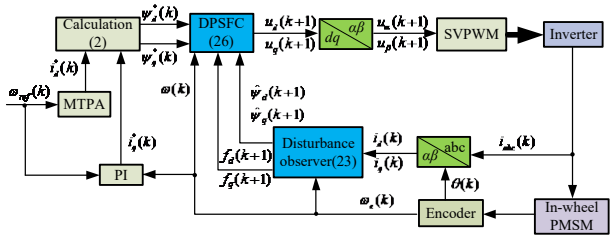

Fig. 8. Block diagram of the DPSFC with disturbance observer method.

V. Simulation Results and Analysis

To validate the system performance with the proposed DPSFC approach, simulations of the conventional DPCC method and the DPSFC method have been conducted in MATLAB/Simulink, while the i_d=0 control strategy is adopted. The parameters of the in-wheel PMSMs used in the simulation are listed in Table I. The proposed disturbance observer parameters are K_1 =-400, K_2 =400, K_3 =-400, and K_4 = -400.

The simulation results of the conventional DPCC and the

proposed DPSFC schemes are shown in Figs. 9-14. In the simulation, the control performance of the two control methods has been compared at 360 rpm and 400 rpm with a torque of 25 Nm. For each situation under DPCC method, the flux linkage and flux linkage reference of q-axis are given. The red line represents the flux linkage, and the purple line represents its reference. For each situation under DPSFC method, two curves are given. They are, from top to bottom, the flux linkage and flux linkage reference of q-axis, and the estimated disturbance of d-axis and q-axis, respectively. The comparison reults which show the specific values of the flux linkage response error rate and the estimated disturbance under all conditions in the simulations have been listed in Table II.

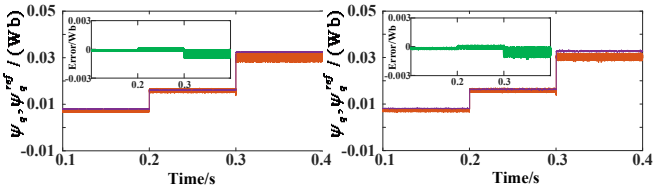

Fig. 9. Flux linkage responses of the conventional DPCC with inductance mismatches: (a) 360rpm and 25Nm, and (b) 400rpm and 25Nm.

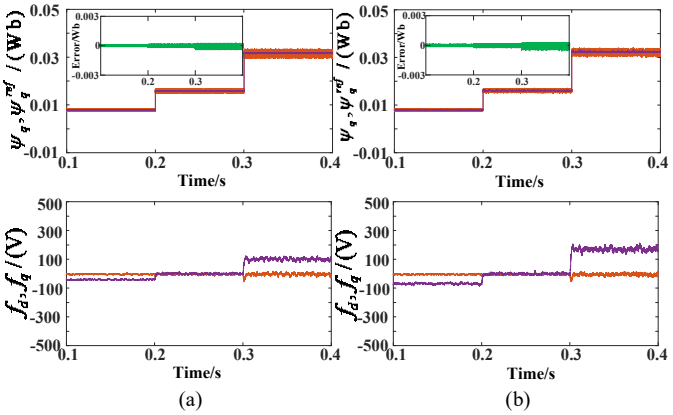

Fig.10. Flux linkage responses and the estimated disturbances of the proposed DPSFC with inductance mismatches: (a) 360rpm and 25Nm, and (b) 400rpm and 25Nm.

The flux linkage responses under inductance mismatches and the zoomed-in flux linkage response error plots are depicted in the Figs. 9 and 10. From 0.1 s to 0.2 s, the inductance value is half of its initial value, and the inductance value is twice its initial value from 0.3 s to 0.4 s ($0.5L_s \rightarrow L_s \rightarrow 2L_s$). Figs. 11 and 12 show the flux linkage responses under permanent magnet flux mismatches and their zoomed-in flux linkage response error plots. The permanent magnet flux value is half of its initial value from 0.1 s to 0.2 s, and twice its initial value from 0.3 s to 0.4 s ($0.5\psi_f \rightarrow \psi_f \rightarrow 2\psi_f$). As shown, the proposed DPSFC shows a better performance than the conventional method. The actual flux linkage value of q-axis of DPCC cannot track its reference accurately when the inductance mismatches or the permanent magnetic flux mismatches occur. In addition, the tracking error increases with respect to speed. The disturbances of d- and q-axes caused by inductance mismatches or the permanent magnetic flux mismatches, estimated from disturbance observer and feedbacked to DPSFC, are depicted in Figs.10 and 12.

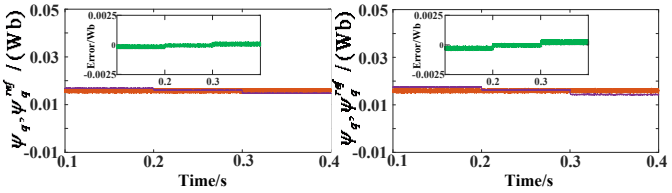

Fig. 11. Flux linkage responses of the conventional DPCC with permanent magnet flux mismatches: (a) 360rpm and 25Nm, and (b) 400rpm and 25Nm.

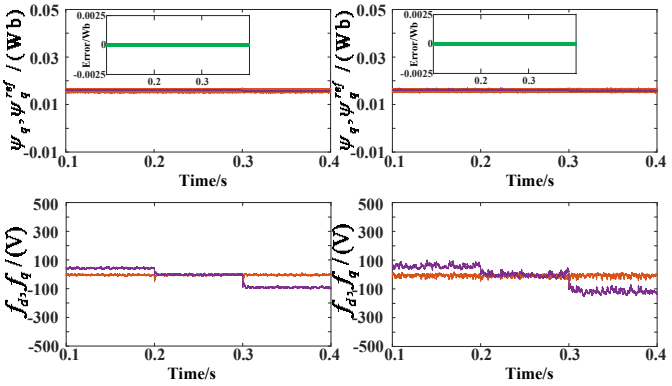

Fig. 12. Flux linkage responses and the estimated disturbances of the proposed DPSFC with permanent magnet flux mismatches: (a) 360rpm and 25Nm, and (b) 400rpm and 25Nm.

It can be found in Fig.10 that the positive q-axis compensation voltage is generated from 0.3 s to 0.4 s because the flux linkage value of q-axis is smaller than the reference flux value. Consequently, the error between the actual value of flux linkage and its reference is reduced. Meanwhile, a larger disturbance of q-axis is produced at 400 rpm, to be specific, -78 V at 400 rpm and -40 V at 360 rpm whenΔL_s =-0.5L_s, 190 V at 400 rpm and 100 V at 360 rpm when $\Delta L_s = L_s$, which can also indicate that the error increases with respect to speed. In the simulations, the i_d=0 control strategy is adopted so that there exists little effect on the d-axis flux linkages.

It can be observed in Fig. 12 that the negative q-axis compensation voltage is generated from 0.3 s to 0.4 s because the flux linkage value of q-axis is bigger than the value of reference flux. Meanwhile, a larger disturbance of q-axis is produced at 400rpm, to be specific, 60 V at 400 rpm and 45 V at 360 rpm when$\Delta\psi_f$ =-0.5ψ_f, -115 V at 400 rpm and -80 V at 360 rpm when$\Delta\psi_f$ =ψ_f, which can also indicate that the error increases with speed. As a result, the error between the actual value of flux linkage and its reference is narrowed.

Figs. 13 and 14 illustrate the flux linkage responses and the zoomed-in flux linkage response error plots under inductance and permanent magnet flux mismatches. The combined parameter mismatches changed in the span from 0.1s to 0.5s as: $0.5L_s$+$0.5\psi_f \rightarrow 2L_s$+$0.5\psi_f \rightarrow 2L_s$+$2\psi_f \rightarrow 0.5L_s$+$2\psi_f$. As shown, the proposed DPSFC method can offer better performance in terms of tracking the reference flux linkage. The actual flux linkage value of q-axis of DPCC cannot track its reference accurately when the inductance and permanent magnet flux mismatches occur. In addition, the tracking error also increases with speed which can be found through disturbance curves. A larger disturbance of q-axis is produced at 400 rpm, which can also

indicate that the error increases with speed. The disturbances of d- and q-axes caused by the inductance and permanent magnetic flux mismatches estimated by disturbance observer, feedbacked to DPSFC, are utilized to compensate the voltage resulting in a reduced error between the actual value of flux linkage and its reference.

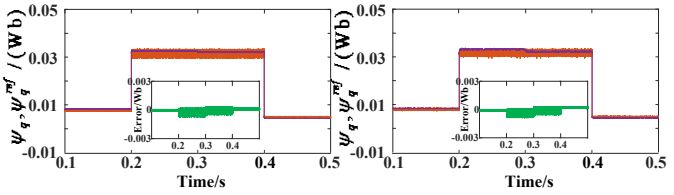

(a) (b)

Fig. 13. Flux linkage responses of the conventional DPCC with inductance and permanent magnet flux mismatches: (a) 360rpm and 25Nm, and (b) 400rpm and 25Nm.

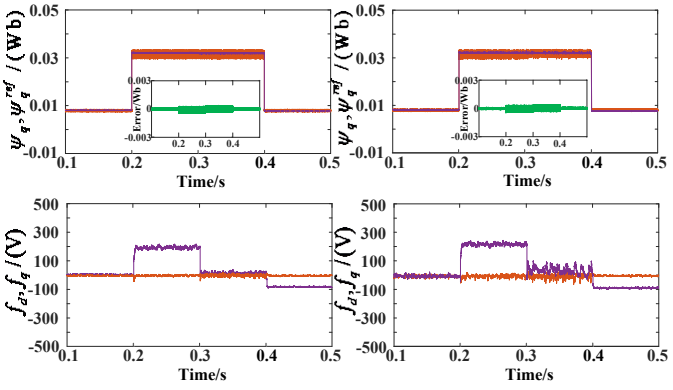

(a) (b)

Fig. 14. Flux linkage responses and the estimated disturbances of the proposed DPSFC with inductance and permanent magnet flux mismatches: (a) 360rpm and 25Nm, and (b) 400rpm and 25Nm.

TABLE II
COMPARISON RESULTS IN SSIMULATION

	Parameter mismatches	DPCC	Proposed DPSFC	
		Flux linkage response error rate	Flux linkage response error rate	Estimated disturbance
360rpm +25Nm	ΔL_s=-0.5L_s	2.05%	1.2%	-40V
	ΔL_s=L_s	3.06%	0.9%	100V
	$\Delta\psi_f$=-0.5ψ_f	2%	1.24%	45V
	$\Delta\psi_f$=ψ_f	2.63%	0.6%	-80V
	ΔL_s=-0.5L_s+ $\Delta\psi_f$=-0.5ψ_f	2.5%	1.25%	4V
	ΔL_s=L_s+ $\Delta\psi_f$=-0.5ψ_f	3.6%	1.21%	191V
	ΔL_s=L_s+ $\Delta\psi_f$=ψ_f	1.61%	0.6%	12V
	ΔL_s=-0.5L_s+ $\Delta\psi_f$=ψ_f	2.97%	1.2%	-81V
400rpm +25Nm	ΔL_s=-0.5L_s	2.22%	1.25%	-78V
	ΔL_s=L_s	5.1%	1.24%	190V
	$\Delta\psi_f$=-0.5ψ_f	2.35%	1.24%	60V
	$\Delta\psi_f$=ψ_f	2.98%	0.63%	-115V
	ΔL_s=-0.5L_s+ $\Delta\psi_f$=-0.5ψ_f	2.91%	1.62%	-7V
	ΔL_s=L_s+ $\Delta\psi_f$=-0.5ψ_f	4.13%	1.51%	215V
	ΔL_s=L_s+ $\Delta\psi_f$=ψ_f	2.61%	0.63%	34V
	ΔL_s=-0.5L_s+ $\Delta\psi_f$=ψ_f	3.12%	1.23%	-89V

VI. EXPERIMENT RESULTS

Fig. 15 shows the experimental setup and the scheme of the hardware implementation. The test bench consists of an in-wheel PMSM, a torque sensor, and a magnetic powder brake. The system parameters are the same as those listed in Table I. The proposed control scheme is experimentally implemented in a dSPACE 1401 test bench. The experimental measurements are exported from the dSPACE platform for analysis. The in-wheel PMSM model in the host computer is turned into C code automatically in dSPACE 1401. Then, 0-1 digital signals from dSPACE are sent into signal conditioning board. Subsequently, the PWM waves generated from the signal conditioning board can control the switch of the IGBT. Finally, the three phase currents are outputted to control the in-wheel PMSM. Meanwhile, the current and position signals are fed back to dSPACE to realize the closed loop control. Since the rated parameter could not be changed randomly in the experiments, the parameter variation was realized in the DPSFC controller (dSPACE1401).

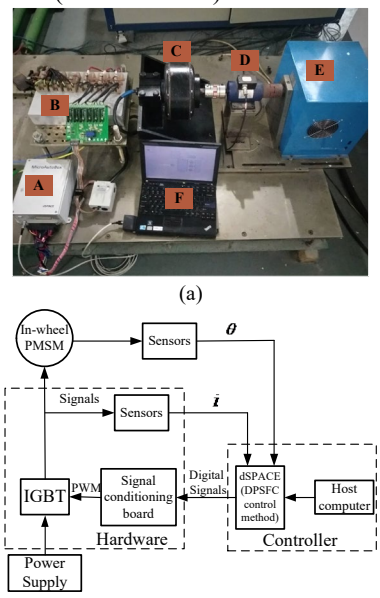

(a)

(b)

Fig. 15. (a) Experimental platform of the PMSM system (A: dSPACE, B:Inverter, C: in-wheel PMSM, D: Torque sensor, E: Magnetic powder brake, and F: Host computer), and (b) the scheme of the hardware implementation.

Similar to the simulations, the experimental results of the conventional DPCC and the proposed DPSFC schemes are shown in Figs. 16-21. In the experiment, the control performances of the two control methods have been compared at 360 rpm and 400 rpm with a torque of 25 Nm. For each situation under DPCC method, flux linkage and flux linkage reference of q-axis are given. The purple line represents the flux linkage and the blue line represents its reference. For each situation under DPSFC method, two curves are given. They are, from top to bottom, the q-axis flux linkage response and its reference (the purple line represents the flux linkage and the blue line represents its reference), the estimated disturbance of d-axis and q-axis (The purple line represents d-axis disturbance and the blue line represents q-axis disturbance), respectively.

The flux linkage responses under inductance mismatches ($0.5L_s \rightarrow L_s \rightarrow 2L_s$) and the zoomed-in flux linkage response error

plots are given in Figs. 16 and 17. The flux linkage responses under permanent magnetic flux mismatches ($0.5\psi_f \rightarrow \psi_f \rightarrow 2\psi_f$) are shown in Figs. 18 and 19, as well as the zoomed-in flux linkage response error plots. The flux linkage responses under the combined inductance and permanent magnet flux parameter mismatches ($0.5L_s+0.5\psi_f \rightarrow 2L_s+0.5\psi_f \rightarrow 2L_s+2\psi_f \rightarrow 0.5L_s+2\psi_f$) and their zoomed-in error plots are shown in Figs. 20 and 21. As shown, the proposed DPSFC has better performance than the conventional method. The actual flux linkage value of q-axis of DPCC cannot track its reference accurately when the inductance mismatches occur. Similar to the simulation results, it can be found that a larger disturbance of q-axis is produced at 400 rpm than at 360 rpm, which also indicates that the tracking error increases with speed. The estimated disturbance is used to compensate for the voltage. That is, the error between the actual value of flux linkage and its reference is reduced due to the compensated voltage. The comparison reults which show the specific values of the flux linkage response error rate and the estimated disturbance under all conditions in the experiments have been listed in Table III.

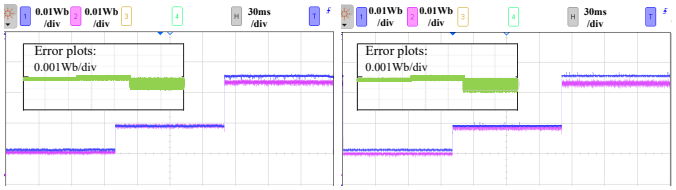

(a) (b)

Fig. 16. Flux linkage responses of the conventional DPCC with inductance mismatches: (a) 360rpm and 25Nm, and (b) 400rpm and 25Nm.

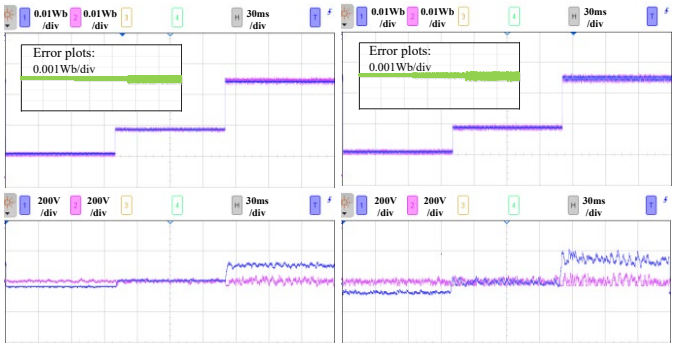

(a) (b)

Fig. 17. Flux linkage responses and the estimated disturbances of the proposed DPSFC with inductance mismatches: (a) 360rpm and 25Nm, and (b) 400rpm and 25Nm.

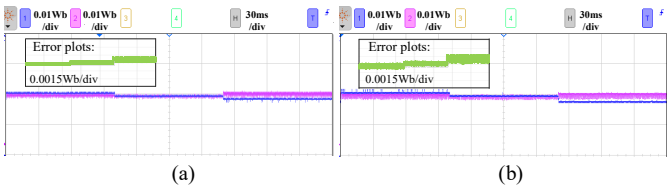

(a) (b)

Fig. 18. Flux linkage responses of the conventional DPCC with permanent magnet flux mismatches: (a) 360rpm and 25Nm, and (b) 400rpm and 25Nm.

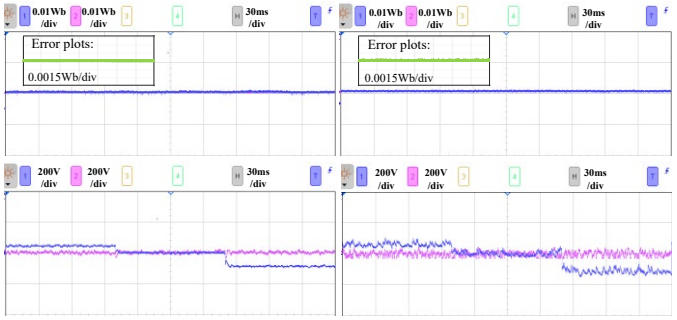

(a) (b)

Fig. 19. Flux linkage responses and the estimated disturbances of the proposed DPSFC with permanent magnet flux mismatches: (a) 360rpm and 25Nm, and (b) 400rpm and 25Nm.

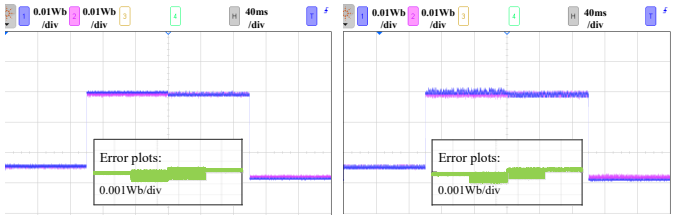

(a) (b)

Fig. 20. Flux linkage responses of the conventional DPCC with inductance and permanent magnet flux mismatches: (a) 360rpm and 25Nm, and (b) 400rpm and 25Nm.

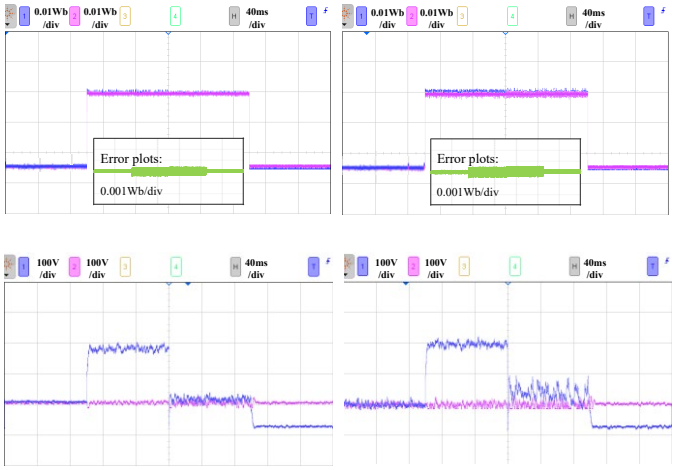

(a) (b)

Fig. 21. Flux linkage responses and the estimated disturbances of the proposed DPSFC with inductance and permanent magnet flux mismatches: (a) 360rpm and 25Nm, and (b) 400rpm and 25Nm.

TABLE III
COMPARISON RESULTS IN EXPERIMENTS

	Parameter mismatches	DPCC	Proposed DPSFC	
		Flux linkage response error rate	Flux linkage response error rate	Estimated disturbance
360rpm +25Nm	ΔL_s=-0.5L_s	2.35%	1.21%	-45V
	ΔL_s=L_s	3.56%	0.91%	105V
	$\Delta\psi_f$=-0.5ψ_f	2.94%	1.24%	45V
	$\Delta\psi_f$=ψ_f	2.71%	0.6%	-87V
	ΔL_s=-0.5L_s+ $\Delta\psi_f$=-0.5ψ_f	2.57%	1.73%	5V
	ΔL_s=L_s+ $\Delta\psi_f$=-0.5ψ_f	3.15%	1.68%	196V
	ΔL_s=L_s+	1.72%	0.6%	17V

	$\Delta\psi_f$=ψ_f			
	ΔL_s=-0.5L_s+ $\Delta\psi_f$=ψ_f	3.12%	2.1%	-85V
400rpm +25Nm	ΔL_s=-0.5L_s	3.13%	1.25%	-88V
	ΔL_s=L_s	5.07%	1.25%	188V
	$\Delta\psi_f$=-0.5ψ_f	2.56%	1.29%	69V
	$\Delta\psi_f$=ψ_f	3.07%	0.63%	-126V
	ΔL_s=-0.5L_s+ $\Delta\psi_f$=-0.5ψ_f	3.61%	3.52%	-6V
	ΔL_s=L_s+ $\Delta\psi_f$=-0.5ψ_f	4.96%	2.19%	221V
	ΔL_s=L_s+ $\Delta\psi_f$=ψ_f	2.83%	0.73%	58V
	ΔL_s=-0.5L_s+ $\Delta\psi_f$=ψ_f	3.22%	2.23%	-93V

VII. Conclusion

In this paper, an improved DPSFC method with disturbance observer has been proposed for in-wheel PMSM drives under low-speed condition. The influence of parameter mismatch on the conventional DPCC has been analyzed in detail. Since the DPCC is a model-based control strategy, the control performance will deteriorate when parameter mismatch exists due to the temperature rise, magnet demagnetization and other faults, especially for the in-wheel PMSM whose heat dissipation performance is not good. To address the problem, a disturbance observer was designed to predict the stator flux linkage in the next period and estimate the disturbance caused by parameter mismatch simultaneously. The predicted stator flux linkage of the next period is used to replace the current flux to compensate for the one-step delay in digital control, and the estimated disturbance is to compensate for the output voltage in the DPSFC method. The proposed DPSFC method can effectively improve the robustness against parameter mismatch and the tracking errors, which has been proved theoretically and also has been verified by simulation and experimental results. The compromise between less calculation burden and better control performance will be considered in the future. Meanwhile, the sensorless control strategy applied in the DPCC will be further studied.

References

[1] F. J. Anayi and M. M. A. Al Ibraheemi, "Estimation of rotor position for permanent magnet synchronous motor at standstill using sensorless voltage control scheme, " *IEEE/ASME Trans. Mechatron.*, vol. 25, no. 3, pp. 1612-1621, Jun. 2020.

[2] X. Sun, Z. Shi, G. Lei, Y. Guo, and J. Zhu, "Analysis and design optimization of a permanent magnet synchronous motor for a campus patrol electric vehicle," *IEEE Trans. Veh. Technol.*, vol. 68, no. 11, pp. 10535-10544, Nov. 2019.

[3] Y. Lee, L. Sun, J. Moon, C. C. Chung and M. Tomizuka, "Reference modulation for performance enhancement of motion control systems with nonlinear parameter variations, " *IEEE/ASME Trans. Mechatron.*, vol. 24, no. 5, pp. 2040-2051, Oct. 2019.

[4] X. Sun, Z. Shi, G. Lei, Y. Guo, and J. Zhu, "Multi-objective design optimization of an IPMSM based on multilevel strategy," *IEEE Trans. Ind. Electron.*, vol. 68, no. 1, pp. 139-148, Jan. 2021.

[5] S. K. Kommuri, Y. Park and S. B. Lee, "On-line compensation of mechanical load defects with composite control in PMSM drives, " *IEEE/ASME Trans. Mechatron.*, doi: 10.1109/TMECH.2020.3019507.

[6] F. Bu, *et al.*, "Rotor position tracking control for low speed operation of direct-drive PMSM servo system, " *IEEE/ASME Trans. Mechatron.*, doi: 10.1109/TMECH.2020.3019039.

[7] X. Sun, C. Hu, G. Lei, Y. Guo, and J. Zhu, "State feedback control for a PM hub motor based on grey wolf optimization algorithm," *IEEE Trans. Power Electron.*, vol. 35, no. 1, pp. 1136-1146, Jan. 2020.

[8] Z. Shi, X. Sun, Y. Cai, and Z. Yang, "Robust design optimization of a five-phase PM hub motor for fault-tolerant operation based on Taguchi method," *IEEE Trans. Energy Convers.*, vol. 35, no. 4, pp. 2036-2044. Dec. 2020.

[9] Y. Mao, S. Zuo, and J. Cao, "Effects of rotor position error on longitudinal vibration of electric wheel system in in-wheel PMSM driven vehicle," *IEEE/ASME Trans. Mechatron.*, vol. 23, no. 3, pp. 1314-1325, Jun. 2018.

[10] Z. Shi, X. Sun, G. Lei, Z. Yang, Y. Guo, and J. Zhu, "Analysis and optimization of radial force of permanent magnet synchronous hub motors," *IEEE Trans. Magn.*, vol. 56, no. 2, Feb. 2020, Art. no.: 7508804.

[11] W. Jiang, P. Wang, Y. Ni, J. Wang, L. Wang, and Y. Liao, "Multimode current hysteresis control for brushless DC motor in motor and generator state with commutation torque ripple reduction," *IEEE Trans. Ind. Electron.*, vol. 65, no. 4, pp. 2975-2985, Apr. 2018.

[12] X. Sun, J. Cao, G. Lei, Y. Guo, and J. Zhu, "A composite sliding mode control for SPMSM drives based on a new hybrid reaching law with disturbance compensation," *IEEE Trans. Transport. Electrific.*, 2021, DOI: 10.1109/TTE.2021.3052986.

[13] T. Tarczewski and L. M. Grzesiak, "Constrained state feedback speed control of PMSM based on model predictive approach," *IEEE Trans. Ind. Electron.*, vol. 63, no. 6, pp. 3867-3875, Jun. 2016.

[14] X. Sun, J. Cao, G. Lei, Y. Guo, and J. Zhu, "A robust deadbeat predictive controller with delay compensation based on composite sliding mode observer for PMSMs," *IEEE Trans. Power Electron.*, 2021, DOI: 10.1109/TPEL.2021.3063226.

[15] Y. Luo and C. Liu, "Elimination of harmonic currents using a reference voltage vector based-model predictive control for a six-phase PMSM motor," *IEEE Trans. Power Electron.*, vol. 34, no. 7, pp. 6960-6972, Jul. 2019.

[16] M. Wu, et al, "Improved model predictive torque control for PMSM drives based on duty cycle optimization," *IEEE Trans. Magn.*, vol. 57, no. 2, Feb. 2021, Art. no.: 8200505.

[17] Y. Luo and C. Liu, "Model predictive control for a six-phase PMSM motor with a reduced-dimension cost function," *IEEE Trans. Ind. Electron.*, vol. 67, no. 2, pp. 969-979, Feb. 2020.

[18] J. A. Suul, K. Ljokelsoy, T. Midtsund, and T. Undeland,"Synchronous reference frame hysteresis current control for grid converter applications," *IEEE Trans. Ind. Appl.*, vol. 47, no. 5, pp. 2183-2194, Sep.-Oct. 2011.

[19] H. H. Choi, H. M. Yun, and Y. Kim, "Implementation of evolutionary fuzzy PID speed controller for PM synchronous motor," *IEEE Trans. Ind. Inf.*, vol. 11, no. 2, pp. 540-547, Apr. 2015.

[20] L. Chen, et al, "Three-vector-based model predictive torque control for a permanent magnet synchronous motor of EVs," *IEEE Trans. Transport. Electrific.*, 2021. DOI: 10.1109/TTE.2021.3053256.

[21] X. Sun, M. Wu, G. Lei, Y. Guo, and J. Zhu, "An improved model predictive current control for PMSM drives based on current track circle," *IEEE Trans. Ind. Electron.*, vol. 68, no. 5, pp. 3782-3793, May 2021.

[22] W. Xie, *et al*., "Finite-control-set model predictive torque control with a deadbeat solution for PMSM drives," *IEEE Trans. Ind. Electron.*, vol. 62, no. 9, pp. 5402-5410, Sep.2015.

[23] X. Sun, C. Hu, J. Zhu, S. Wang, W. Zhou, Z. Yang, G. Lei, K. Li, B. Zhu, and Y. Guo, "MPTC for PMSMs of EVs with multi-motor driven system considering optimal energy allocation," *IEEE Trans. Magn.*, vol. 55, no. 7, pp. 1-6, Jul. 2019, Art. no. 8104306.

[24] X. Zhang, L. Zhang, and Y. Zhang, "Model predictive current control for PMSM drives with parameter robustness improvement," *IEEE Trans. Power Electron.*, vol. 34, no. 2, pp. 1645-1657, Feb. 2019.

[25] X. Zhang, B. Hou, and Y. Mei, "Deadbeat predictive current control of permanent-magnet synchronous motors with stator current and disturbance observer," *IEEE Trans. Power Electron.*, vol. 32, no. 5, pp. 3818-3834, May 2017.

[26] X. Yuan, C. Zhang, and S. Zhang, "A novel deadbeat predictive current control scheme for OEW-PMSM drives," *IEEE Trans. Power Electron.*, vol. 34, no. 12, pp. 11990-12000, Dec. 2019.

[27] S. Kang, J. Soh, and R. Kim, "Symmetrical three-vector-based model predictive control with deadbeat solution for IPMSM in rotating reference frame," *IEEE Trans. Ind. Electron.*, vol. 67, no. 1, pp. 159-168, Jan. 2020.

[28] Y. Wang, *et al*., "Deadbeat model-predictive torque control with discrete space-vector modulation for PMSM drives," *IEEE Trans. Ind. Electron.*, vol. 64, no. 5, pp. 3537-3547, May 2017.
[29] A. M. Aljehaimi and P. Pillay, "Novel flux linkage estimation algorithm for a variable flux PMSM," *IEEE Trans. Ind. Appl.*, vol. 54, no. 3, pp. 2319-2335, May-June 2018.
[30] Y. Yao, Y. Huang, F. Peng, J. N. Dong, and H. Zhang, "An improved deadbeat predictive current control with online parameter identification for surface-mounted PMSMs," *IEEE Trans. Ind. Electron.*, DOI: 10.1109/TIE.2019.2960755.
[31] X. Yuan, S. Zhang, and C. Zhang, "Enhanced robust deadbeat predictive current control for PMSM drives," *IEEE Access*, vol. 7, pp. 148218-148230, 2019.
[32] Y. Jiang, W. Xu, C. Mu, and Y. Liu, "Improved deadbeat predictive current control combined sliding mode strategy for PMSM drive system," *IEEE Trans. Veh. Technol.*, vol. 67, no. 1, pp. 251-263, Jan. 2018.
[33] G. Pei, J. Liu, X. Gao, W. Tian, L. Li, and R. Kennel, "Deadbeat predictive current control for SPMSM at low switching frequency with moving horizon estimator," *IEEE J. Emerg. Sel. Top. Power Electron.*, DOI: 10.1109/JESTPE.2019.2960579.
[34] L. Springob and J. Holtz, "High-bandwidth current control for torque ripple compensation in PM synchronous machines," *IEEE Trans. Ind. Electron.*, vol. 45, no. 5, pp. 713–721, Oct. 1998.

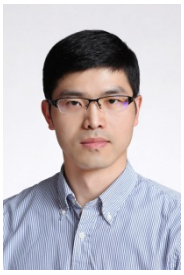

Xiaodong Sun (M'12-SM'18) received the B.Sc. degree in electrical engineering, and the M.Sc. and Ph.D. degrees in control engineering from Jiangsu University, Zhenjiang, China, in 2004, 2008, and 2011, respectively.

Since 2004, he has been with Jiangsu University, where he is currently a Professor in Vehicle Engineering with the Automotive Engineering Research Institute. From 2014 to 2015, he was a Visiting Professor with the School of Electrical, Mechanical, and Mechatronic Systems, University of Technology Sydney, Sydney, Australia. His current teaching and research interests include electrified vehicles, electrical machines, electrical drives, and energy management. He is the author or coauthor of more than 100 refereed technical papers and one book, and he is the holder of 42 patents in his areas of interest. Dr. Sun is an Editor of the IEEE TRANSACTIONS ON ENERGY CONVERSION.

Yao Zhang was born in Yancheng, Jiangsu, China, in 1997. She received the B.S. degree in vehicle engineering from Jiangsu University, Zhenjiang, China, in 2018, and she is currently working toward the M.Sc. degree in Jiangsu University, Zhenjiang, China.

Her current research interests include modeling, structure designing and controlling of permanent magnet synchronous motors for electric vehicle propulsion.

Gang Lei (M'14) received the B.S. degree in Mathematics from Huanggang Normal University, China, in 2003, the M.S. degree in Mathematics and Ph.D. degree in Electrical Engineering from Huazhong University of Science and Technology, China, in 2006 and 2009, respectively.

He is currently a Senior Lecturer at the School of Electrical and Data Engineering, University of Technology Sydney (UTS), Australia. His research interests include computational electromagnetics, design optimization and control of electrical drive systems and renewable energy systems. He is an Associate Editor of the IEEE TRANSACTIONS ON INDUSTRIAL ELECTRONICS and an Editor of the IEEE TRANSACTIONS ON ENERGY CONVERSION.

Youguang Guo (S'02-M'05-SM'06) received the B.E. degree from Huazhong University of Science and Technology, China in 1985, the M.E. degree from Zhejiang University, China in 1988, and the Ph.D. degree from University of Technology Sydney (UTS), Australia in 2004, all in electrical engineering.

He is currently a Professor at the School of Electrical and Data Engineering, UTS. His research fields include measurement and modeling of properties of magnetic materials, numerical analysis of electromagnetic field, electrical machine design optimization, power electronic drives and control.

Jianguo Zhu (S'93–M'96–SM'03) received the B.E. degree in 1982 from Jiangsu Institute of Technology, Jiangsu, China, the M.E. degree in 1987 from Shanghai University of Technology, Shanghai, China, and the Ph.D. degree in 1995 from the University of Technology Sydney (UTS), Sydney, Australia, all in electrical engineering.

He was appointed a lecturer at UTS in 1994 and promoted to full professor in 2004 and Distinguished Professor of Electrical Engineering in 2017. At UTS, he has held various leadership positions, including the Head of School for School of Electrical, Mechanical and Mechatronic Systems and Director of Centre for Electrical Machines and Power Electronics. In 2018, he joined the University of Sydney, Australia, as a full professor and Head of School for School of Electrical and Information Engineering. His research interests include computational electromagnetics, measurement and modelling of magnetic properties of materials, electrical machines and drives, power electronics, renewable energy systems and smart micro grids.